Human Molecular Genetics, 2021, Vol. 30, No. 8 629–643

doi: 10.1093/hmg/ddab065
Advance Access Publication Date: 9 March 2021
General Article

GENERAL ARTICLE

Calcium is reduced in presynaptic mitochondria of motor nerve terminals during neurotransmission in SMA mice

Mario Lopez-Manzaneda, Julio Franco-Espin, Rocio Tejero, Raquel Cano and Lucia Tabares*,†

Department of Medical Physiology and Biophysics, School of Medicine, University of Seville, 41009 Seville, Spain

*To whom correspondence should be addressed at: Department of Medical Physiology and Biophysics, School of Medicine, University of Seville, Avda. Sánchez Pizjuán, 4 41009 Seville, Spain, Tel: +34 954 55 6574; Email: ltabares@us.es

Abstract

Spinal muscular atrophy (SMA) is an autosomal recessive degenerative motor neuron disease characterized by symmetrical muscle weakness and atrophy of limb and trunk muscles being the most severe genetic disease in children. In SMA mouse models, motor nerve terminals display neurotransmitter release reduction, endocytosis decrease and mitochondria alterations. The relationship between these changes is, however, not well understood. In the present study, we investigated whether the endocytosis impairment could be related to the functional alteration of the presynaptic mitochondria during action potential (AP) firing. To this aim, we generated a Synaptophysin-pHluorin (SypHy) transgenic mouse, crossed it with Taiwanese SMA mice, and recorded exo- and endocytosis and mitochondria Ca^{2+} signaling in real-time at *ex vivo* motor nerve terminals of Taiwanese-SypHy mice. The experiments were performed at the beginning of the motor symptoms to get an integrated view of the nerve terminal's functional state before degeneration. Our electrophysiological and live imaging results demonstrated that the mitochondria's capacity to increase matrix-free Ca^{2+} in SMA mice was significantly limited during nerve AP firing, except when the rate of Ca^{2+} entry to the cytosol was considerably reduced. These results indicate that both the mitochondrial Ca^{2+} signaling alterations and the secretion machinery defects are significant players in the dysfunction of the presynaptic terminal in SMA.

Introduction

Spinal muscular atrophy (SMA) is an autosomal recessive neuromuscular disease, the leading genetic cause of infant mortality (1). The disease is characterized by the loss of lower motor neurons, muscle weakness and paralysis. SMA is produced by homozygous mutations or loss of the *SMN1* (survival of motor neuron 1) gene resulting in null expression of the SMN protein (2). A homologous gene, *SMN2*, which exons differ from *SMN1* in a single nucleotide—a cytosine (C) to a thymine (T) in exon 7—produces truncated SMN and a small, and frequently insufficient, amount of full SMN. SMN protein is implicated in multiple house-keeping functions, including small nuclear ribonucleoprotein (snRNP) biogenesis, pre-mRNA splicing and ribosome regulation (3,4).

In SMA mouse models, motor nerve terminals display both neurotransmitter release decrease (5–8) and endocytosis defects

†Lucia Tabares, http://orcid.org/0000-0002-4027-4044
Received: December 29, 2020. **Revised:** February 21, 2021. **Accepted:** February 23, 2021

(9–12). Mitochondrial structure and metabolism are also altered (6,8,13,14). For example, mitochondria are less abundant (15) and have reduced length (14) than in controls. In NSC-34 cells, an inducible drop of SMN decreases ATP levels and increases cytochrome c activity (16). Additionally, in SMN-deficient spinal motoneurons, mitochondrial bioenergetics-related genes are dysregulated, the respiration rate and ATP synthesis are reduced, and the oxidative stress level increased (14,16).

Normally, through the uptake of Ca^{2+} from the cytosol, synaptic mitochondria both regulate cytosolic Ca^{2+} signaling locally and precisely adapt ATP production to energetic demands. The concentration of free Ca^{2+} in the mitochondrial matrix depends on its influx, efflux and buffering by inorganic phosphate (Pi). Ca^{2+} enters the matrix through the mitochondrial channel uniporter (MCU) (17–19) following the electrochemical gradient generated across its inner membrane. The inside-negative mitochondrial membrane potential (Ψ_m), in turn, is created by proton extrusion across the inner membrane coupled to the activity of the electron transport chain (ETC), which is subsequently harnessed by the ATP synthase in the production of ATP. Cytosolic Ca^{2+} enters the mitochondria following its entry from the extracellular medium through voltage-dependent calcium channels (VDCCs), ionotropic receptors coupled to G proteins, or its release from the endoplasmic reticulum (ER). The ER contacts mitochondria through specialized regions, so-called mitochondria-associate ER membrane (MAM) (20). Ca^{2+} extrusion occurs in neurons mainly by the sodium-calcium exchanger (NCLX) (21). Disturbance in one or more of these elements could lead to mitochondrial Ca^{2+} overload or deficit. Thus, we wondered whether the exo- and endocytosis defects in motor nerve terminals coexist in time with an alteration in presynaptic mitochondria Ca^{2+} handling and, if so, by which mechanism the synaptic vesicle cycle could be affected by the mitochondria impairment.

To address these questions, we generated a variant of the Taiwanese SMA mouse line that expresses the genetically encoded fusion protein synaptophysin-pHlourin (SypHy). This mouse line permits studying exo- and endocytosis simultaneously in real-time. The same mouse line was used to monitor mitochondrial Ca^{2+} at rest and during electrical activity. Our findings provided an integrated view of the impairment of the exo–endocytosis cycle and revealed that presynaptic mitochondria's ability to handle activity-induced Ca^{2+} loads was altered in SMA motor nerve terminals.

Results

Neurotransmission impairment in SMA terminals

To better understand the motor terminal functional state in SMA mice, we investigated neurotransmission by different technical approaches, namely, electrophysiology, immunohistochemistry and dynamic imaging of exo-endocytosis.

First, we recorded endplate potentials with glass microelectrodes to determine the number of quanta released in our mouse model. Figure 1A shows representative traces of the endplate potentials (EPPs) in control and SMA littermate mice, as well as mean EPP amplitudes, mean miniature endplate sizes and mean number of quanta released per AP (quantal content, QC) recorded at 0.5-Hz nerve stimulation (bar graphs). While the mean size of the EPPs was similar in SMA mice and control littermates (mutants: 32.68 ± 5.04 mV, 13 fibers, 5 mice; controls: 29.65 ± 4.16 mV; 19 fibers, 5 mice), the miniature EPPs (mEPPs) were significantly larger in SMA (2.59 ± 0.29 mV) than in control mice (1.72 ± 0.18 mV) ($P = 0.6$ and 0.008, respectively, U-Mann–Whitney test). QC was 29.4% decreased in mutants (12.08 ± 0.87) in comparison with controls (17.13 ± 1.59) ($P = 0.009$, U-Mann–Whitney test). These data indicate a clear decrease in secretion, together with an increase in the input resistance of the muscular fibers in the Taiwanese SMA mice.

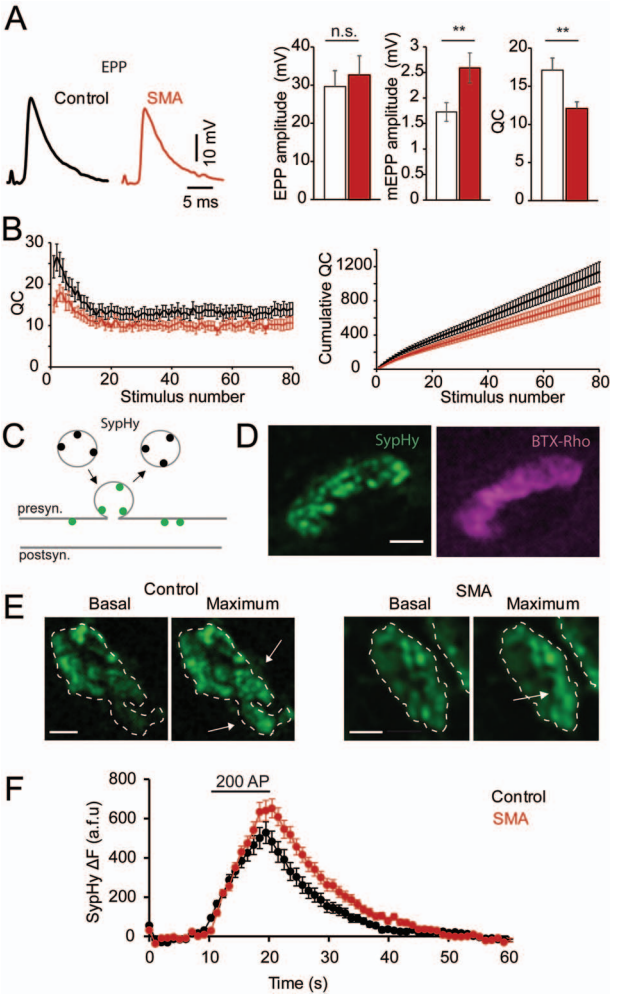

Figure 1. Exo- and endocytosis impairment in SMA motor nerve terminals. (**A**) Representative EPP recordings, and mean EPP, mEPP and QC values in control (black) and SMA (red) mice. (**B**) Number of quanta (left graph) and cumulative quanta (right graph) released during a train of stimuli at 20 Hz in control and SMA terminals. Control: 14 fibers, four experiments; SMA: 11 fibers, four experiments. (**C**) Diagram of the states of SypHy. When the intravesicular medium is acidic, SypHy is quenched (black spots), but when the fusion pore opens, the alkaline medium of the synaptic cleft makes SypHy bright (green spots). After endocytosis, the vesicle acidifies again, and the fluorescence progressively decreases to the basal level. (**D**) Live-imaging of an NMJ expressing SypHy at the nerve terminal (left) and in which the postsynaptic side was stained with bungarotoxin conjugated to rhodamine (BTX-Rho, right). Scale bar: 5 µm. (**E**) Images of SypHy fluorescence signals from a control and an SMA terminal (outlined) at rest (basal) and at the end of electrical stimulation (maximum). The arrows indicate areas of greater intensity during stimulation. In the SMA images, note that a second terminal is partially seen in the field (upper right corner) and responds to the stimulus. Calibration bars: 5 µm. (**F**) Mean SypHy fluorescence increment in control (53 terminals, nine mice) and SMA (45 terminals, five mice) before, during and after 200 AP (horizontal bar).

The kinetics of EPPs—determined by the time course of neurotransmitter release, the passive electrical properties of the postsynaptic membrane, and the molecular characteristics of the postsynaptic receptors—was prolonged in SMA (rise time: 1.07 ± 0.08 ms; decay time constant: 4.8 ± 0.59 ms) compared

with control mice (rise time: 0.92 ± 0.09 ms; decay time constant: 3.5 ± 0.2 ms) ($P = 0.033$ and 0.0038, respectively, *U*-Mann–Whitney test), in agreement with previous results in SMAΔ7 motor nerve terminals (5,7,8).

At high-stimulation frequency (20 Hz), we monitored how the release (QC) changed during a train of 100 APs. In both, control and SMA mice, the number of quanta released per AP increased during the first few stimuli (facilitation), followed by a progressive decrease until reaching a plateau level (short-term depression) (Fig. 1B, left graph). In SMA terminals, however, the release was significantly lower than in control littermates. For example, after 80 AP (Fig. 1B, right graph), the mean number of quanta released was 1265.9 ± 189.6 in controls, but only 865.9 ± 91.1 in SMA what represents a 32% decrease of exocytosis ($P = 0.04$; two-tails *t*-test, unpaired). With longer stimulation trains, the percentage decrease was similar since the amplitude of the plateau remained constant in both genotypes, as described before (5,7,8).

Second, we explored whether the Taiwanese-SypHy SMA mouse model presented altered levels of the synaptic proteins synaptotagmin 1 and 2 (Syt1 and Syt2), and synaptic vesicle protein 2B (SV2B), as the SMNΔ7 mutant mice do (7,22). Syt2 is the primary Ca^{2+} sensor for exocytosis at motor nerve terminals and SV2 is a multi-functional protein belonging to the major facilitator superfamily transporters and has been proposed to participate in cell Ca^{2+} homeostasis (23), to regulate the size of the readily releasable pool of vesicles (24), and contribute to the endocytosis of Syt (25).

We performed immunohistochemistry for Syt1, Syt2 and SV2B proteins and performed confocal quantitative imaging analysis. We found a statistically significant reduction in the postsynaptic area in comparison with controls, quantified by bungarotoxin-rhodamine staining (Supplementary Material, Fig. S1A), as well as a decrease in SV2B (48 ± 3%), and Syt2 (38 ± 5%, Supplementary Material, Fig. S1B) area ($P < 0.0005$; *U*-Mann–Whitney test). Conversely, the mean fluorescent surface area for Syt1 in mutants was 75 ± 2.5% higher than in controls ($P < 0.0005$; *U*-Mann–Whitney test), as in SMNΔ7 mice, probably due to the delay in switching from Syt1 to Syt2 in the nerve terminals of the transversus abdominis anterior (TVA) muscle (7,22). Nevertheless, the reduction of the proteins in the Taiwanese model was less pronounced than in SMNΔ7 mice, in good correlation with a minor neurotransmission deficit in the Taiwanese (30%) than in the SMNΔ7 mouse (50%) (5). Thus, these findings reinforce the hypothesis that the Syt2 and SV2B decrease is likely associated with the presynaptic SMA pathology. The results also suggest that the neurotransmission defects in SMA mice may have multiple origins, not surprising given the number of molecules and pathways potentially affected by the decrease of SMN.

Third, we studied the degree of affectation of the synaptic vesicle cycle by optically monitoring exo- and endocytosis in real-time (26–28). The technique used relies on synaptic vesicles carrying pHluorin molecules, a modified GFP whose fluorescence is pH-dependent. The pHlourin is quenched by protonation in the acidic vesicle lumen, then unquenched upon exocytosis when exposed to the more alkaline extracellular medium, and quenched again following endocytosis and reacidification (Fig. 1C) (26–28). Figure 1D shows an example of a nerve terminal expressing SypHy (left image) and its postsynaptic side (right image), stained after adding BTX-Rhodamine to the chamber.

Figure 1E displays typical examples of SypHy fluorescence before (basal) and at the end (maximum) of a train of 200 AP at 20 Hz, in terminals of both genotypes. Figure 1F shows the mean fluorescence experimental values obtained in control (black) and SMA (red) terminals. The amplitude of the fluorescent increment during the AP train reflects the balance between exocytosis and endocytosis. Since we already confirmed that exocytosis is decreased in our SMA model (Fig. 1A and B), one should expect a smaller SypHy response in SMA than in controls, unless an additional defect in endocytosis–reacidification exists.

The basal fluorescence of the terminals was very similar in both genotypes; however, the peak fluorescent increment (ΔF) was about 20% larger in SMA (722.4 ± 52 a.f.u., *n*, *N*: 45, 5) than in control terminals (602.3 ± 60.6 a.f.u., *n*, *N*: 53, 9) ($P < 0.0047$, Mann–Whitney test) (Fig. 1F), indicating less endocytosis–reacidification during the stimulation train. After the stimulation train, the decay time constants were not different (τ: 10.6 ± 0.7 s; *n*, *N*: 45, 5) than in controls (τ: 9.9 ± 0.7 s; *n*, *N*: 53, 9), ($P = 0.3$, Mann–Whitney test).

Mitochondria are essential for exo–endocytosis in SMA motor nerve terminals

Neurotransmitter release and vesicle recycling via endocytosis depend on ATP availability (29). In particular, endocytosis is one of the first processes to be compromised in the absence of energy (30). Since mitochondria are defective in SMA motor neurons (6,8,13,14), we wondered whether glycolysis could be homeostatically upregulated in SMA motor nerve terminals to compensate for the possible ATP deficit via oxidative phosphorylation.

To investigate it, we compared the peak amplitudes and the relaxation time constants of the SypHy fluorescent responses with and without glucose in the extracellular solution (10 and 0 mM, respectively). In the last, glucose was replaced by extracellular pyruvate (1.25 mM) and lactate (1.25 mM) as substrates for ATP mitochondrial production.

In control terminals, the mean peak fluorescence was slighter higher with 0 mM than with 10 mM glucose (722.4 ± 52, and 602.3 ± 60.6 a.f.u., respectively, $P = 0.01$, *U*-Mann–Whitney test) (Fig. 2A and B). In SMA terminals, they were not different (721.4 ± 58.2, and 722.4 ± 52 a.f.u., respectively; $P = 0.87$, *U*-Mann–Whitney test). The time constant of relaxation was significantly slower in 0 mM than in 10 mM glucose (15.5 ± 1 and 9.9 ± 0.7 s, respectively, $P = 0.0001$, *U*-Mann–Whitney test) in control terminals, but not different in SMA terminals (9.6 ± 0.6 s and 10.6 ± 0.7 s, $P = 0.4$, *U*-Mann–Whitney test).

These results show that exo–endocytosis in control motor nerve terminals have a significant but relatively small sensitivity to extracellular glucose. At the same time, SMA terminals were insensitive to glucose retrieval. In both cases, they signaled that the primary source of ATP during the synaptic vesicle cycle is the mitochondria, in clear contrast to what occurs in central synapses in which ATP synthesis by glycolysis is critical (30).

We next confirmed that the exo–endocytosis–reacidification cycle in mutant nerve terminals was dependent on oxidative phosphorylation. To do so, we added to the 0 mM glucose solution oligomycin (5 μg/ml), which blocks mitochondrial ATP production by direct inhibition of the ATP synthase. Figure 2C (left panel) shows two representative recordings from the same terminal before (red trace) and after 35 min in oligomycin (blue trace). With oligomycin, the response was significantly smaller and stayed high after the stimuli ended. To better compare the endocytosis process's slowdown, the right graph in Figure 2C shows overlays of the same traces after normalizing the blue trace to the red one. Subsequent stimulation trains produced no further active responses and a progressive increase in mitochondrial basal fluorescence (Fig. 2D), indicating the cessation of both the exocytosis and the endocytosis–reacidification processes in the absence of ATP synthesis by the mitochondria.

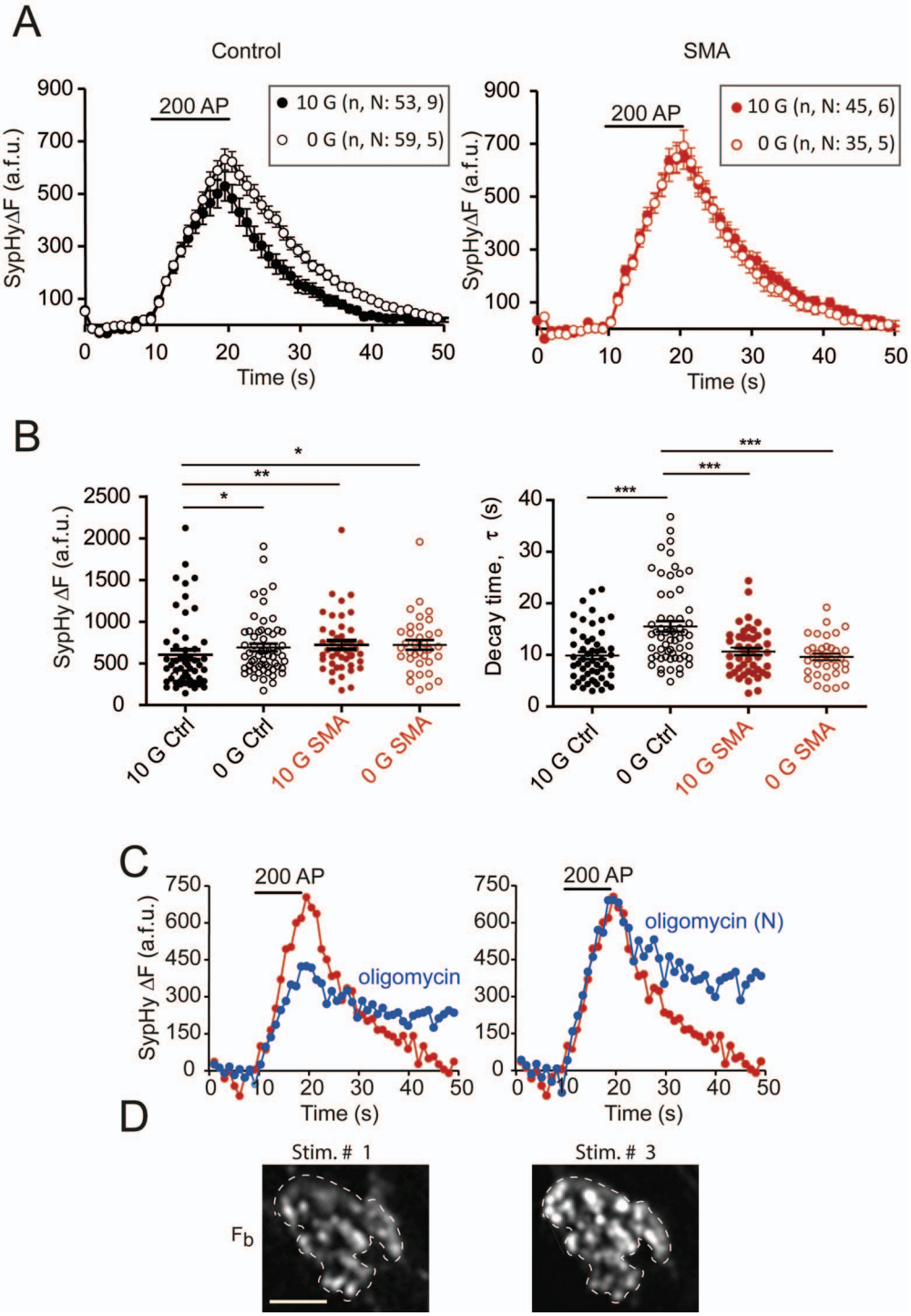

Figure 2. Exo- and endocytosis in SMA terminals is highly dependent on mitochondrial ATP production. (**A**) Time course of the mean SypHy fluorescence signals during 200 stimuli at 20 Hz in control (left graph) and SMA terminals (right graph), in the presence of 10 mM glucose (filled symbols) or in the absence of glucose (open symbols). Extracellular glucose was replaced by 1.25 mM pyruvate plus 1.25 mM lactate. (**B**) Fluorescence peak increments (left) and decay time constants from the terminals represented in (**A**). (**C**) Left panel: Representative example of the response of a terminal to 200 AP (horizontal bar) before (red trace) and after (blue trace) 35 min in oligomycin. Note that the blockage of the mitochondrial ATP synthesis decreases the peak amplitude of the signal and slows the recovery after the stimulation train. Right panel: Same traces, but after normalization of blue trace amplitude to the red one. (**D**) Representative example of the SypHy basal fluorescence (F_b) of a nerve terminal before a first stimulus train (left) and a third train (right) separated by 10 min. Note the increase in basal fluorescence in the right image, which also explains the lack of response to the third stimulation in the presence of oligomycin. Calibration bar: 5 µm.

Characteristics of the mitochondrial calcium signals at perinatal age

Since, to our knowledge, no direct information exists about SMA synaptic mitochondria's capacity to increase matrix-free Ca^{2+} during electrical nerve activity, a mechanism essential to synthesize ATP on demand, we investigated whether Ca^{2+} signaling was changed at motor nerve presynaptic mitochondria.

The features of the presynaptic mitochondrial Ca^{2+} signals at 1-week-old mice, the age at which SMA mice present synaptic dysfunction at motor nerve terminals (7), however, have not been described before. Then, we first characterized the spatial and temporal characteristics of the mitochondrial Ca^{2+} responses in control mice using Rhod-2 AM (5 μM). The acetoxymethyl (AM) ester group of the dye, which facilitates its cellular uptake, is removed by intracellular esterases resulting in the selective accumulation of Rhod-2 within mitochondria.

At rest, Rhod-2 fluorescence in control presynaptic motor nerve terminals at near-physiological temperature (30–32°C) was low, as illustrated in Figure 3A (upper and lower left panels). However, upon Ca^{2+} entry into the terminal by a brief electrical nerve stimulation train (100 action potentials, AP), 3–12 bright spots rapidly appeared (Fig. 3A, central panels). After the stimuli ceased, the fluorescence decayed slowly until reaching the resting level (Fig. 3A, right panels) (Supplementary Material Supplementary Movie). The analysis of the time course of the intensity change during the stimuli (Fig. 3B) shows that the signal increased to a maximum amplitude maintained constant (plateau) for the rest of the train. When the stimulation stopped, the signal decayed slowly back towards its resting level. The average rising time ($t_{10–90}$) of the signal in control terminals was 1.47 ± 0.15 s, and the half-decay time ($t_{1/2}$) 19.7 ± 1.04 s what represents a 13-fold difference in kinetics. Qualitatively, the observed response did not differ from the mitochondrial transients already described at adult motor nerve terminals (31) and other cell types (32,33).

To confirm the mitochondrial origin of the signal, we exposed the preparation to carbonyl cyanide m-chlorophenylhydrazone (CCCP). This protonophore abolishes the Ψ_m and depletes mitochondrial Ca^{2+}. Before CCCP, we added to the bath solution oligomycin (5 μg/ml) to minimize the ATP depletion associated with the reverse action of the ATP synthase (complex V) during the CCCP application (34). Figure 3C and D shows a terminal's responses in the absence of the drugs (black trace and left panels, respectively) and after 5 min with 1 μM CCCP (gray trace and right panels). After CCCP, the response to the stimulation train much disappeared, remaining only a CCCP-resistant component characterized by a fast decay indicating its cytosolic origin (35). Under these experimental conditions, the relatively large cytosolic Ca^{2+} signal may result from the mitochondria's inability to sequester Ca^{2+}, which is reported by non-dialyzed residual Rhod-2 in the cytosol.

To estimate the sensitivity of perinatal presynaptic mitochondria in motor nerve terminals to cytosolic Ca^{2+} increments, we measured the matrix-free Ca^{2+} fluorescent signal rise as a function of the stimulus strength. Figure 3E shows an example of the mitochondrial responses in a single terminal stimulated with 25 and 50 AP. Figure 3F displays the mean amplitude of the responses (27 terminals) as a function of the number of AP. Remarkably, the mean fluorescence reached about 18% of its maximum with only seven AP, i.e., 350 ms after starting the stimulation. Half-rise was reached after 12–13 AP (600 ms from the beginning), and the plateau amplitude was reached with approximately 50 impulses (after 2.5 s from the start). These results demonstrate that mitochondria in presynaptic motor terminals at perinatal age begin to uptake Ca^{2+} very fast upon repetitive nerve stimulation, suggesting they have a high calcium sensitivity.

Besides the typical mitochondrial responses (Fig. 3B), two other types of stimuli-locked fluorescent signals sporadically appeared within the same terminal (Supplementary Material, Fig. S2A). One, characterized by its fast-rising and decaying phases (Supplementary Material, Fig. S2C), and the other by a fast-slow biphasic decaying (Supplementary Material, Fig. S2D). These two signals' kinetics were consistent with a pure cytosolic Ca^{2+} transient and a cytosolic-mitochondrial mixed response, respectively (34). Additionally, in a few terminals, bright and unresponsive spots were identified (Supplementary Material, Fig. S2E). In the experiments presented here, only areas displaying the typical monotonic slow decay of pure mitochondrial responses (Supplementary Material, Fig. S2B) were considered for further analysis.

Mitochondrial matrix free calcium is reduced in SMA motor terminals

Next, we compared mitochondrial matrix-free Ca^{2+} levels in control and SMA terminals of littermate mice at postnatal days 6–8, both at rest and during an AP train.

At rest, mitochondrial Ca^{2+} fluorescence was low and stable in both genotypes (Fig. 4A). The mean basal fluorescence was 1013 ± 121.5 a.f.u.; n, $N = 26$, 8 in controls, and 745 ± 90 a.f.u.; n, $N = 22$, 6 in SMA; ($P = 0.14$; U-Mann–Whitney test) (Fig. 4B), indicating that cytosolic Ca^{2+} is not altered in SMA nerve terminals in the absence of electrical activity.

Then, we assessed whether mitochondrial free Ca^{2+} level in SMA was similar to controls during repetitive electrical activity (100 AP, 20 Hz). On average, the fluorescence raised 3.1-fold ±0.3 in controls and 1.8-fold ±0.2 in mutants ($P = 0.004$; U-Mann–Whitney test) (Fig. 4C and D) what represents a 42% lower plateau response in SMA compared with controls. Furthermore, in mutants, only 32% of the terminals had F_{max} higher than 2000 a.f.u. (Fig. 4E, red symbols), in contrast with 81% of control terminals (Fig. 4E, black symbols).

Since the plateau level could be affected by the probe's saturation by Ca^{2+}, we checked this possibility. We first recorded a mitochondrial response in 2 mM Ca^{2+} external solution (Fig. 4F, R1) and then switched to one with no calcium added. After 45 min, we applied digitonin to permeabilize the plasma membrane, and the basal fluorescence measured again (Fig. 4F, R2). Finally, we switched back to 2 mM Ca^{2+} and measured the fluorescence once again. At this point, a substantial increase in fluorescence was recorded (Fig. 4F, R3), indicating that the probe was not saturated during the plateau, in accordance with previous results (36).

Once the dye saturation was ruled out, we estimated the correlation between the fluorescence intensity and matrix-free Ca^{2+} values in control and mutant with the Grynkiewicz's equation (37)

$$\left[Ca^{2+}\right] = Kd\ \left[(F - F\,min) / (F\,max - F)\right])$$

where F_{min} was obtained in free-Ca^{2+} bath solution and F_{max} at saturated Ca^{2+} concentration in the presence of 40 μg/ml of digitonin. Assuming a K_D of Rhod-2 of 570 nM, we estimated that the apparent matrix-free Ca^{2+} concentration during the plateau was approximately 1.18 μM in control and 0.69 μM in mutants. Remarkably, the mean value obtained in 1-week-old controls was

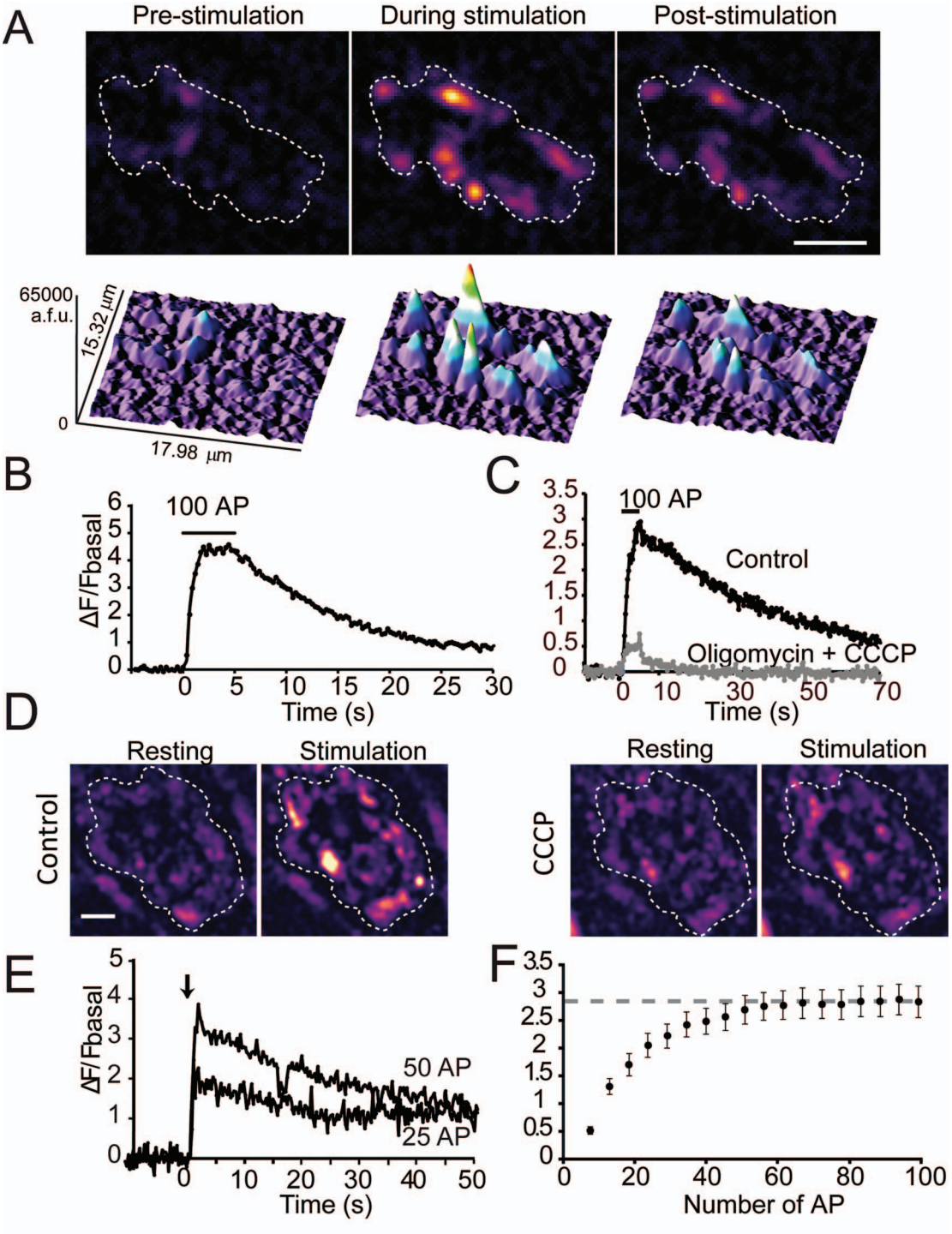

Figure 3. Transitory rise of mitochondrial calcium following depolarization-induced Ca^{2+} entry in motor nerve terminals at P7. (**A**) 2D (upper panels) and 3D (lower panels) spatial images of mitochondrial calcium fluorescence signals before, during and after a train of 100 AP (20 Hz) at a typical presynaptic terminal. Scale bar: 5 µm. The color scale represents the amplitude of the responses. (**B**) Temporal representation of fluorescence increase ($\Delta F/F_{basal}$) during stimulation (black horizontal line) at 20 Hz, during 5 s, from a terminal in control conditions. (**C**) Response of the same terminal before (black trace) and after (gray trace) applying the mitochondrial depolarizing agent CCCP (1 µM) in the presence of oligomycin (5 µg/ml). Note the substantial decrease in the calcium signal and the change in kinetics. (**D**) Images from the terminal represented in C, at rest, and the end of the stimulation, in the absence or not of CCCP and oligomycin. Scale bar: 5 µm. (**E**) Example of the mitochondrial responses to 25 and 50 AP in a terminal. The arrow indicates the beginning of the stimuli. (**F**) Relationship between the number of AP and the amplitude of mitochondrial calcium signals (mean of 27 terminals, from 9 experiments). In (**A** and **D**), the terminals are outlined.

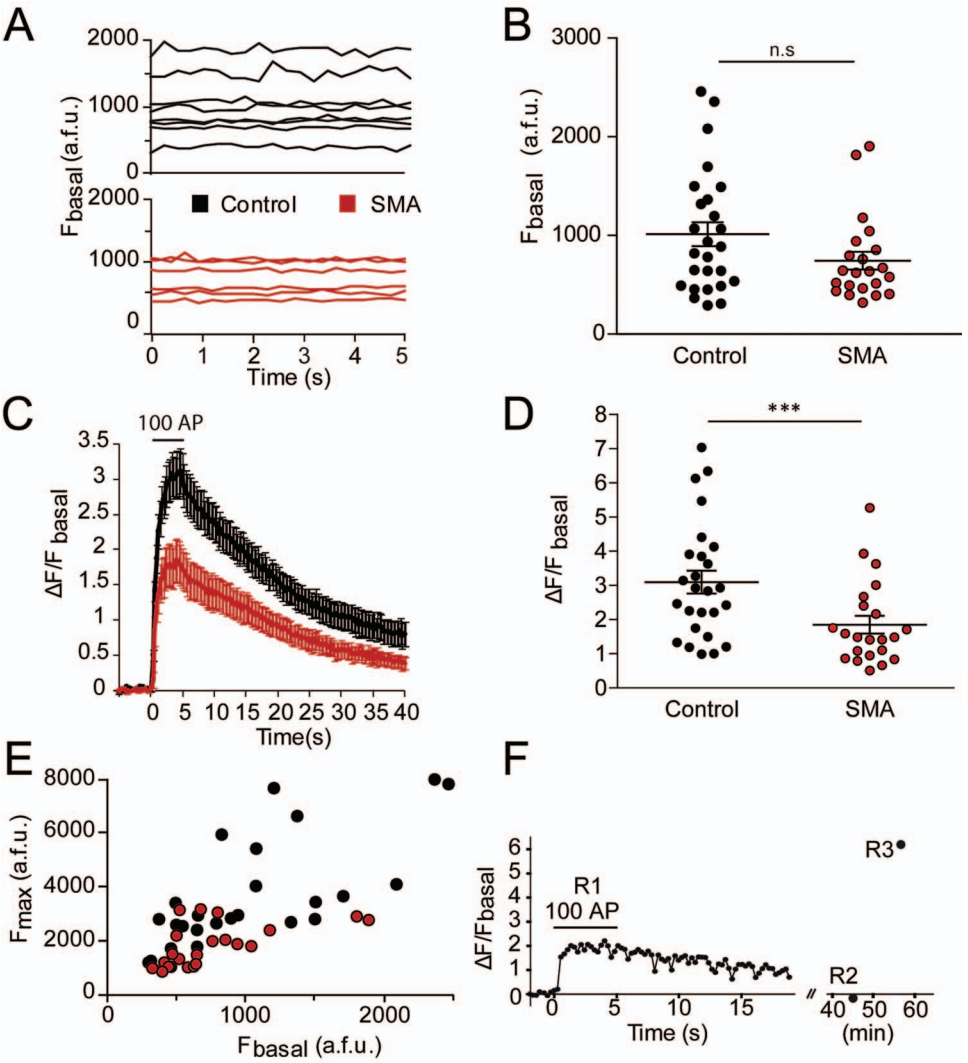

Figure 4. Mitochondrial calcium rise during AP firing is impaired in SMA motor terminals. (**A**) Basal calcium levels are stable before stimulation in both genotypes. Each trace represents the mitochondrial signals from a different motor terminal. (**B**) Mean basal fluorescence values per terminal show no statistical differences between genotypes ($P = 0.14$; *U*-Mann–Whitney test (control: 26 terminals, eight experiments; SMA: 22 terminals, six experiments). (**C**) Mean responses of free mitochondrial calcium before, during and after stimulation (100 AP, 20 Hz), normalized to basal values in control and SMA motor nerve terminals. The horizontal bar indicates the stimulation interval. (**D**) Mean peak increments are significantly reduced by 42% in mutants (22 terminals, six experiments) compared with controls (26 terminals, eight experiments); ***$P = 0.004$. *U*-Mann–Whitney test. (**E**) Representation of basal versus maximum fluorescence values for each terminal in (**D**). (**F**) The plateau level reached during a train of AP (R1) is not due to the saturation of the probe, as verified by permeabilization of the membranes with 40 µg/ml digitonin (R3). Digitonin did not change fluorescence in the nominal absence of extracellular Ca^{2+} (R2).

similar to the maximal increase of mitochondrial free Ca^{2+} (1–2 µM) estimated at adult presynaptic motor nerve mitochondria (36,38), as well as in liver and brain mitochondria (39).

Mitochondrial calcium influx rate during the electrical activity is less in SMA

Subsequently, we analyzed the matrix-free Ca^{2+} rise and falling kinetics during and after the electrical stimulation, respectively, in both genotypes.

Although the mean plateau amplitudes were very different in control and SMA (Fig. 5A and B), the fluorescence increase was initially not significantly different in both genotypes (Fig. 5C, first AP). Nevertheless, the responses rapidly diverged as the number of stimuli increased. The representation of the Ca^{2+} rise's velocity versus time revealed an acceleration followed by a deceleration phase during the stimulation train (Fig. 5D). In controls, the maximum speed of rising was 2703.61 ± 247.48 a.f.u./s, while in mutants, it was 35% lower ($P = 0.02$ *t*-Student test, two tails). In both cases, the maximum velocity was reached after 12 AP. These findings indicate that Ca^{2+} influx velocity into the matrix during the electrical activity is reduced in SMA presynaptic mitochondria.

Next, we tested whether the lower plateau amplitude in mutants might also be due to a larger Ca^{2+} efflux from the matrix. A previous report had shown that a reduction in mitochondrial free Ca^{2+} level occurred when the activity of the NCLX increased, for example, by the phosphorylation of the transporter (40). Thus, we compared the fluorescent signal's time course from the end of the stimulation to the point where it recovered the resting level. The graphs in Figure 5E and F show the mean responses in each genotype as absolute values and

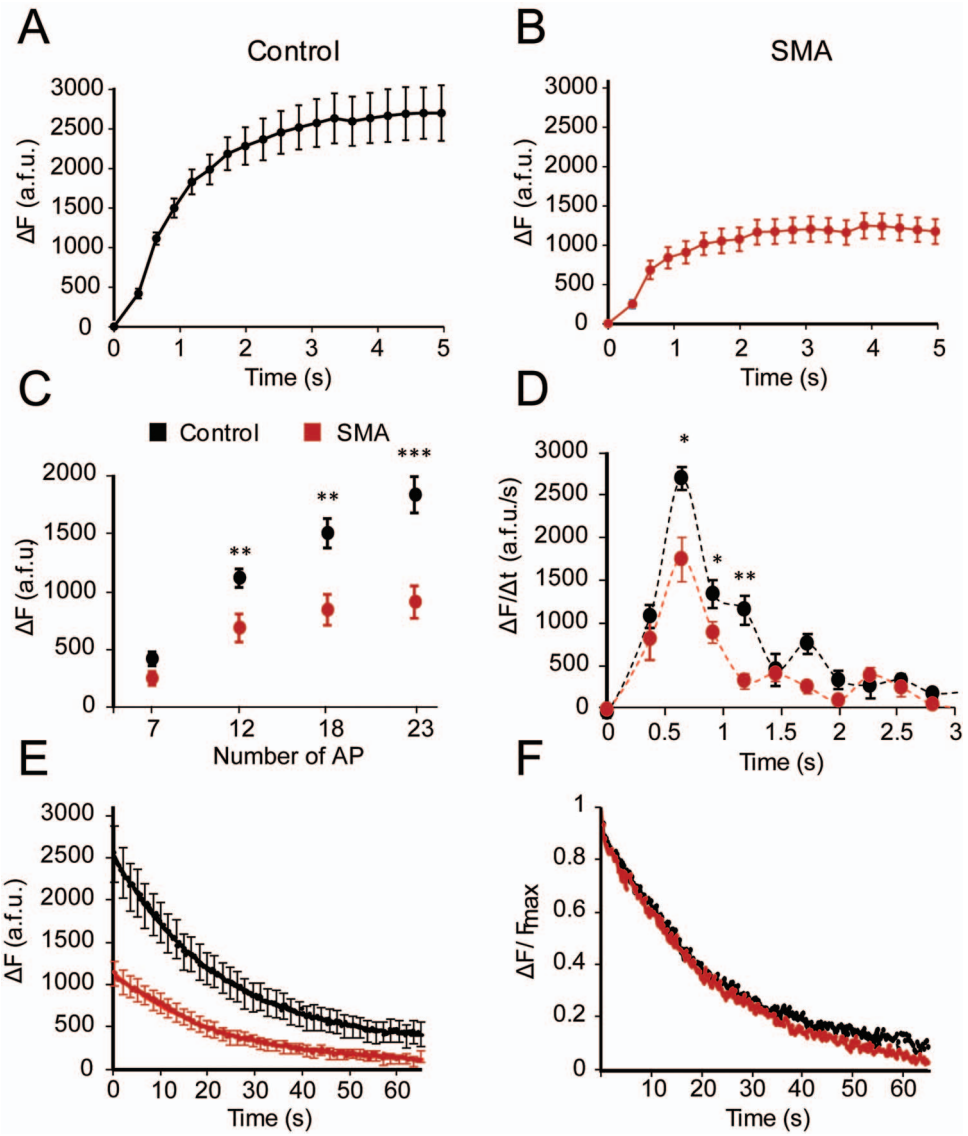

Figure 5. Kinetics of calcium influx in SMA presynaptic mitochondria is slower. (**A**-**B**) Mean fluorescence responses (ΔF) of control (**A**) and SMA (**B**) mitochondria during 100 AP. Note the difference in the plateau amplitudes. (**C**) The amplitudes of the fluorescence responses of control and SMA mitochondria are not significantly different ($P = 0.08$) at the beginning of the stimulation (7 AP) but differ progressively with longer stimulations (12, 18 and 23 AP) (**: 0.0028; ***: <0.0008; *t*-test, two tails). (**D**) The plot of the velocity of the fluorescence change versus time during the first 3 s of stimulation shows the acceleration and deceleration phases of the responses during the rising phase. The acceleration is not different between genotypes with few stimuli but soon becomes significantly lower in mutants ($P = 0.02$; *t* Student). The deceleration phase show significantly higher velocities in control mitochondria (* $P = 0.03$; *U*-Mann–Whitney test, ** $P = 0.0013$ *t* Student). (**E**-**F**) The temporal course of mitochondrial calcium efflux after a 100 AP train at 20 Hz is similar in both genotypes, as evidenced after the amplitude normalization of the fluorescence signals (**F**). Control: 26 terminals, eight experiments; SMA: 22 terminals, six experiments.

after normalization, respectively. The decay half-times were not significantly different between groups (19.7 ± 1.04 s in control and 21.5 ± 2.6 s in SMA; $P = 0.84$; *U*-Mann–Whitney test), indicating that the NCLX functioned similarly. These data also suggest that the efflux rate is independent of the total matrix Ca^{2+} content, as found previously (41).

Mitochondrial membrane depolarization is not responsible for the reduction of matrix Ca^{2+} during the electrical stimulation in SMA terminals

The influx of Ca^{2+} in the matrix might produce an accumulation of positive charges if the extrusion of protons through the ETC did not compensate for it. Thus, we reasoned that the low Ca^{2+} level at the matrix in SMA could be due to Ψ_m depolarization during nerve stimulation. To test this possibility, we incubated the preparation with rhodamine-123 (0.3 μM, 30 min), a fluorescent probe used to measure Ψ_m (42).

In control terminals, we found no significant changes in Ψ_m during the AP train, as illustrated in the representative recording of Figure 6A (left panel). However, as expected, when we added 500 μM 4-AP to the chamber solution, a K^+ channel blocker that prolongs the AP duration and extends Ca^{2+} entry to the cytosol, a large increment in fluorescence was observed (Figure 6A, right panel).

In SMA terminals (Fig. 6B), no change in fluorescence was detected in most cases (left panel), except in a few terminals (4 out of 34) in which an increase in fluorescence was recorded

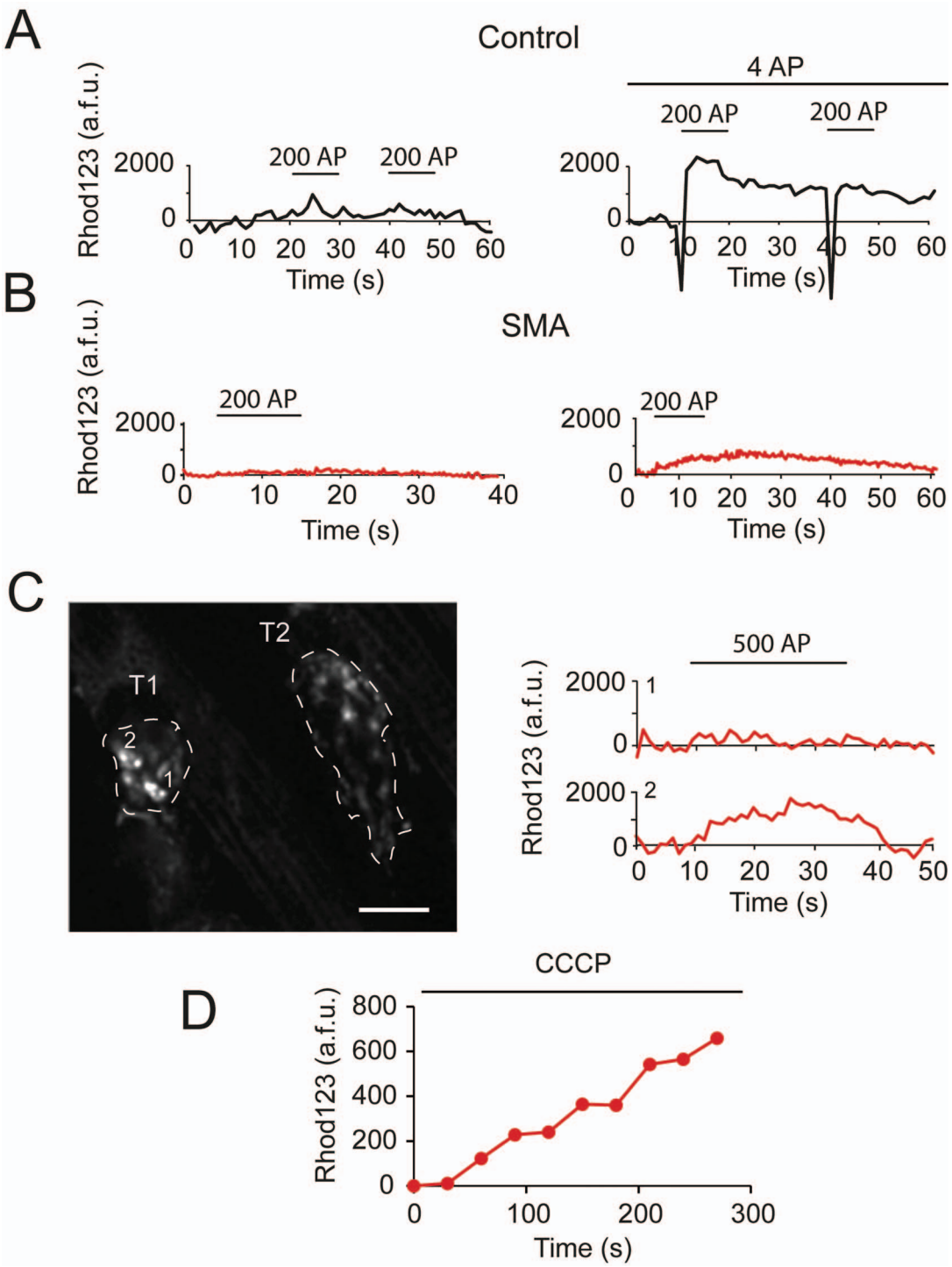

Figure 6. Matrix-free Ca^{2+} reduction in SMA is not due to the depolarization of the mitochondrial membrane potential. (**A**) In nerve terminals from control mice, the fluorescence of rhodamine 123 does not change appreciably during 200 AP trains, as shown in the representative recording of the left panel. However, when the AP duration is prolonged with 4-aminopyridine (4-AP, 500 μM), a transient increase in fluorescence is observed (right graph) in response to the first train; note the downward artifacts at the beginning of the trains due to the powerful contractions produced under this condition. (**B**) In nerve terminals from SMA mice, the fluorescence does not change during 200 AP trains in most terminals (left graph), except in 4 out of 34 recordings, as shown in the example (right graph). (**C**) Left: Image of two nerve terminals (outlined) from an SMA mouse showing six and five fluorescent spots in terminal T1 and T2, respectively. Scale bar: 10 μm. Right: responses of spots number 1 and 2 in T1. No responses were observed in T2. (**D**) The application of the depolarizing agent CCCP (1 μM) slowly increases the fluorescence in mitochondria in the absence of nerve stimulation.

(right panel). The depolarization observed in these few cases was not general for all the mitochondria of the terminal. Figure 6C (left panel) shows two terminals (T1 and T2) from an SMA mouse, in which the stimulation increased the fluorescence in half of the spots (2), but not in the other half (1) of T1, and in none of the five spots in T2. As a control, CCCP was added to the

chamber solution at the end of the experiment, and a progressive increment of fluorescence was evidenced at the same spots (Fig. 6D). Together, these results indicate that the depolarization was a rare event in mutant mitochondria at this age, which discarded this possibility as the cause of the low Ca^{2+} increase in presynaptic mitochondria in SMA mice.

SMA presynaptic mitochondria handle efficiently low calcium influx

Ca^{2+} influx into the mitochondria mainly occurs in excitable cells following the activation of VDCCs at the plasma membrane during nerve activity. Since P/Q-type VDCCs density could be compromised in SMA motor nerve terminals (7,43), we examined whether a decrease in Ca^{2+} influx across the plasma membrane could be responsible for the reduced mitochondrial Ca^{2+} plateau level. To this aim, we compared the amplitude of the mitochondrial signals with 2 mM and low extracellular Ca^{2+} (0.5 mM) solutions in control mice. Remarkably, and in line with previous findings (44,45), the plateau level was the same in both circumstances (Fig. 7A, left panel). However, the time to reach the maximum response was 4.7-fold longer in low calcium. Mean resting mitochondrial free Ca^{2+} was not significantly different in both conditions (Fig. 7A, right panel). These results indicate that the Ca^{2+} concentration gradient across the mitochondrial inner membrane mainly determines the influx's kinetics but not the plateau's amplitude if enough time is given for Ca^{2+} entry. They also suggest that the lower signal in SMA presynaptic mitochondria was not due to a potential decrease of Ca^{2+} entry across VDCCs at the plasma membrane during the electrical activity.

Next, we investigated SMA mitochondria function when the rate of Ca^{2+} entry into the cytosol was lowered. We compared the fluorescence responses with low extracellular Ca^{2+} (0.5 mM) in both genotypes and, surprisingly, found that the fluorescent increments were not significantly different between control (2691 ± 405 a.f.u.) and SMA (2521 ± 352 a.f.u.) terminals ($P = 0.97$, *U*-Mann–Whitney test) (Fig. 7B, left panel). Neither, no significant differences in the rate of Ca^{2+} rise (control: 354 ± 69 a.f.u./s; SMA: 469 ± 84 a.f.u./s; Fig. 7B, right panel), the return kinetics to the basal level (Fig. 7C, left panel), or the efflux rate after stimulation (Fig. 7C, right panel) were observed. These results show that SMA mitochondria, contrarily to the Ca^{2+} uptake saturation observed at physiological conditions (Fig. 5), can handle slow cytosolic Ca^{2+} rises. The determination of the specific mechanism behind the saturation of the Ca^{2+} uptake by the mitochondria is, however, beyond the scope of the present work, as it could go, among other possibilities, from a defect in the expression/function of the MCU channels or in the regulatory proteins of the MCU complex.

Remarkably, the present result is in accordance with our previous finding that neurotransmitter release was not different between control and SMA littermates with 0.5 mM Ca^{2+} at the extracellular solution (7) what indicates, once again, that the motor nerve terminal function well in low Ca^{2+} but cannot handle the physiological extracellular Ca^{2+} concentration.

Discussion

Our *ex vivo* live imaging experiments in SypHy-SMA demonstrate a significant dysfunction in exo- and endocytosis in parallel with the decrease in stimulus-induced Ca^{2+} mitochondrial signals, indicating that the neurotransmission defects in SMA result from interactive changes in the energetic metabolism, Ca^{2+} homeostasis and synaptic proteins network. We now consider various aspects of our main results in more detail.

SMA presynaptic mitochondria has a limited capacity to increase matrix free calcium at the physiological calcium concentration

In some neurodegenerative diseases, mitochondrial Ca^{2+} overload is involved in oxidative stress and caspase 3 activation. However, our experiments showed no Ca^{2+} overload in SMA mitochondria at motor nerve terminals. On the contrary, we found an abnormally low mitochondrial Ca^{2+} plateau level (about 58% of controls) during a train of AP (Fig. 4C and D). Reduction in the mitochondria Ca^{2+} load capacity has been reported before in isolated mitochondria from the spinal cord of fALS mice (46).

We sought to understand the mechanism underlying the reduction in the mitochondrial Ca^{2+} plateau amplitude in SMA for what we considered three scenarios. Namely, that the mitochondria Ca^{2+} entry was decreased, that the Ca^{2+} extrusion from the mitochondria was faster, or that the Ca^{2+} buffering capacity at the matrix was increased.

The reduction of Ca^{2+} entry into the mitochondrial matrix could be due to *a decrease in the Ca^{2+} electrochemical gradient* across the inner membrane. We first wondered whether a drop in the chemical gradient across the mitochondrial membrane, for example, due to a lower Ca^{2+} flow into the cytosol through VDCCs could significantly reduce the mitochondrial plateau. Although P/Q-type VDCCs density seems to be decreased at SMA nerve terminals (7,43,47), our present experiments demonstrate that the mitochondrial plateau amplitude in controls did not change significantly with 2 and 0.5 mM Ca^{2+} in the external solution (Fig. 7A), as also shown before (36,45). Moreover, in controls and mutants, mitochondrial Ca^{2+} increased similarly during the first stimuli (Fig. 5C and D), suggesting a similar initial electrochemical gradient.

Alternatively, we considered an alteration in the electrical gradient. If the accumulation of positive charges in the matrix is not balanced adequately by H^+ extrusion during the electrical activity, a decrease in the electrical driving force (mitochondrial depolarization) may occur. A previous *in vitro* study has reported that Ψ_m in SMA motor neurons is depolarized compared with controls (14). Contrarily, in Smn knock-down NSC34 cells, mitochondrial hyperpolarization has been reported (16). We found no significant alterations in our *ex vivo* measurements with rhodamine-123 when the same stimulation protocol we used to measure the Ca^{2+} plateau (20 Hz, 100–200 AP). These results do not discard, nevertheless, that SMA mitochondria depolarize at later stages of the disease.

In contrast, our experiments indicate that the lower mitochondrial free Ca^{2+} level in SMA terminals during electrical activity is caused by an intrinsic *reduction in the mitochondrial Ca^{2+} influx capacity*. This proposition is sustained by the finding that SMA mitochondria efficiently raised matrix-free Ca^{2+} when the Ca^{2+} cytosolic load was slow (Fig. 7B), but apparently saturated in physiological Ca^{2+} (Figs 4C, D and 5A–D). Interestingly, the rate of Ca^{2+} influx into the mitochondria through the MCU channel is regulated by their respiration capacity (48), which is altered in SMA (14,16). Also, the density of MCU channels and associated proteins are attractive questions for future experiments.

We additionally explored whether the *Ca^{2+} efflux rate* was altered in SMA presynaptic mitochondria due to the dysfunction

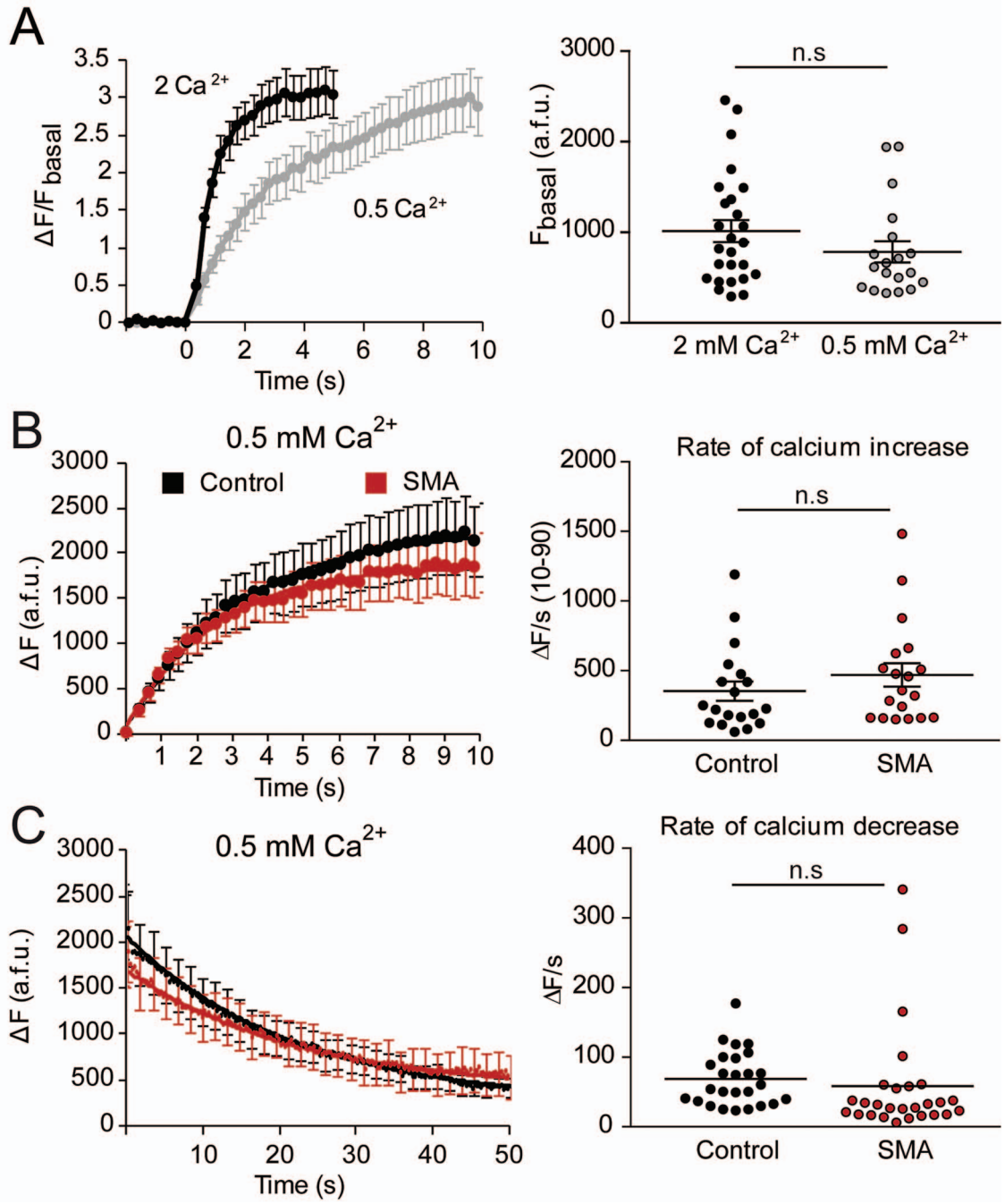

Figure 7. At low extracellular calcium concentration, SMA mitochondria do not show alterations in free calcium. (**A**) Left graph: Reduction of the calcium chemical gradient does not change the mitochondrial Ca^{2+} plateau level. Mean fluorescence increment ($\Delta F/F_{basal}$) versus time with 2 and 0.5 mM extracellular calcium solutions in control terminals. Note that the time to reach the plateau is increased in low calcium, but the plateau level remains the same. Right graph: Basal calcium is not significantly different between conditions ($P = 0.19$; *U*-Mann–Whitney test; 2 mM Ca^{2+}: 26 terminals, eight experiments; 0.5 mM Ca^{2+}: 19 terminals, six experiments). (**B**) Mean amplitude values of mitochondrial free calcium versus time recorded with 0.5 mM Ca^{2+} in the external solution in control and SMA terminals show no differences between genotypes (left panel). The rate of the calcium increase (10–90%) is not different either (right panel). (C) The time course of mitochondrial calcium efflux (left panel) and the rate of calcium decrease, calculated at half of the maximum amplitude, is similar in control and SMA terminals (right panel). Control: 19 terminals, six experiments; SMA: 19 terminals, six experiments.

at the NCLX. However, this possibility was discarded as the time constant of the fluorescent decay after stimulation was similar in both genotypes (Fig. 5E and F).

Finally, we considered whether *Ca^{2+} buffering capacity at the matrix* was increased in SMA. We reasoned that the lower capacity of SMA mitochondria to synthesize ATP (14,16) could produce a higher Pi content at the matrix. However, there were two arguments against it. First, the Pi concentration at the matrix is in equilibrium with the extracellular medium (48). Second, the Ca^{2+} efflux rate is highly dependent on the total Pi concentration (41), and we found no difference in the falling kinetics between controls and mutants (Fig. 5E and F).

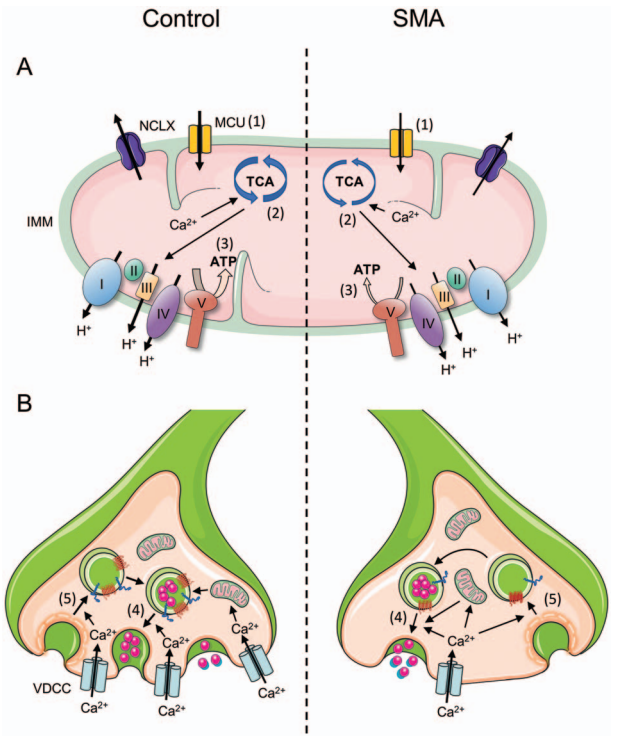

Figure 8. The proposed alteration of the mitochondrial Ca^{2+} homeostasis and its effects on exo- and endocytosis at SMA motor nerve terminals. The discontinuous line at the center separates the control and the SMA situation. (**A**) In control mice, Ca^{2+} influx (1) into the mitochondrial matrix via MCU complexes during AP activity increases the activity of the TCA enzymes (2) and, subsequently, ATP synthesis (3). In SMA mice, Ca^{2+} entry is reduced, which prevents/reduces the corresponding increase in TCA activity and ATP production. (**B**) At motor nerve terminals, exocytosis (4) and endocytosis (5) are activated by Ca^{2+} entry through VDCCs at the plasma membrane. In SMA, the density of VDCCs is apparently decreased, and exocytosis and endocytosis are both impaired. The mitochondrial Ca^{2+} signaling alterations and the reduction of the synaptic vesicle membrane proteins Syt2 (light blue) and SV2B (red) contribute to the dyshomeostasis of the synapse in SMA. Normal function is only achieved with low stimulation. All the graphics elements were taken from the repository https://smart.servier.com/under Creative Commons License 3.0 and modified by us.

Participation of the mitochondria in the dysfunction of the NMJ

In normal conditions, energy production matches cellular needs, and mitochondria play an essential role in it. The stimulation-induced Ca^{2+} load effectively increases ATP production by activating the TCA cycle enzymes (Fig. 8A), which have a $K_{0.5}$ in the range of 0.5–2 μM Ca^{2+} (49,50). In our experiments, the mitochondrial fluorescence elevation was equivalent to a free Ca^{2+} concentration of ~1.18 μM in controls, in agreement with values estimated in adult motor nerve terminals (36). In SMA mice, however, the Ca^{2+} rise was reduced to ~0.69 μM, suggesting a limitation in the capability of the mitochondria to synthesize ATP during repetitive nerve activity, in accord with previous reports of low ATP synthesis in SMA mitochondria (14,16). *Ex vivo* biochemical measurement of the ATP level at the nerve terminals is not possible since ATP's muscle content will contaminate the determination.

How changes in ATP levels impact synaptic function in SMA motor terminals is not known. Here, we hypothesize (Fig. 8B) that part of the defects on exo- and endocytosis are due to the low capacity of SMA mitochondria to increase ATP synthesis during the electrical activity. This proposition is based on three facts: (i) the decrease of the free Ca^{2+} level at the mitochondrial matrix in mutants (Figs 4 and 5), (ii) exo- and endocytosis mostly rely on oxidative ATP production in SMA motor terminals (Fig. 2) and (iii) the synaptic vesicle cycle is the major consumer of ATP at synapses (30).

Nevertheless, given the housekeeping function of SMN, it is expected that, besides ATP, other molecules could be involved in the exocytosis impairment, such as the deficit of Syt2 and SV2B. Regarding endocytosis, also it has been found that the phosphatase activity of calcineurin is decreased in SMA (12), which may produce hyperphosphorylation of proteins involved in endocytosis, such as dynamin 1 (12).

In summary, we demonstrated that *ex vivo* SMA presynaptic mitochondria displayed normal matrix-free Ca^{2+} at rest but reached a significant 42% lower Ca^{2+} level than in controls during neural activity. The defect was due to an altered Ca^{2+} load, independent from a potential reduction in Ca^{2+} entry through VDCCs at the plasma membrane. In contrast, the efflux kinetics of Ca^{2+} from the matrix to the cytosol was not altered. Concomitantly to the above change, real-time experiments of the synaptic vesicle cycle allowed us to characterize the exo- and the endocytosis impairments and prove the relevance of the oxidative production of ATP in the nerve terminal of mutants. Finally, we confirmed that SMA terminals also suffer from a specific reduction in the synaptic proteins Syt2 and SV2B, which are essential for adequate exocytosis at motor nerve synapses. Together, these findings provide a new integrated view of the functional state of the SMA motor nerve terminal before degeneration and indicate that mitochondrial Ca^{2+} signaling alterations contribute to the dyshomeostasis of the synapse.

Material and Methods

Mouse model

We crossed the so-called Taiwanese SMA mice [FVB.Cg-Tg (SMN2)2Hung Smn1tm1Hung/J, stock number 005058] (51) with a mouse line generated at our laboratory that endogenously expresses Synaptophysin-pHluorin (SypHy) in neurons driven by Thy1.2 promoter (https://idus.us.es/bitstream/handle/11441/24203/S_TD_PROV162.pdf?sequence%20=%201&isAllowed%20=%20y). The mice's genotype was identified by PCR. Control mice were heterozygous for the *Smn* gene, while SMA mice were null for *Smn*. Control mice expressing SypHy appeared normal in size, weight and behavior, and the morphology and functionality of their motor nerve terminals were indistinguishable from SypHy negative mice. All recordings were done at the Taiwanese-SypHy line between postnatal days 6 and 8 (P6–8). All experiments were performed according to the guidelines of the European Council Directive for the Care of Laboratory Animals and the animal care and ethics committee of University of Seville.

Acute neuromuscular preparation

Mice were killed by decapitation and exsanguinated. The TVA muscle was dissected with its nerve branches intact and pinned to the bottom of a 2 ml chamber over a bed of cured silicone rubber. Preparations were continuously perfused with a solution of the following composition (in mM): NaCl 135, KCl 4, $CaCl_2$ 2, $MgCl_2$ 1, $NaHCO_3$ 15, NaH_2PO_4 0.33 and glucose 10. The solution was continuously gassed with 95% O_2 and 5% CO_2. For experiments with low extracellular Ca^{2+}, all the procedures, including the dissection, were done in a solution with 0.5 mM Ca^{2+}.

Mitochondrial calcium indicator loading

For the *ex vivo* mitochondrial matrix free calcium assays, we used the membrane-permeable acetoxymethyl ester (AM) form of Rhod-2, Rhod 2-AM (Thermo Fisher Scientific, R1245MP), which compartmentalization is preferentially restricted to the mitochondria. Rhod-2 is a single wavelength Ca^{2+} indicator with peak absorption/emission wavelengths of ∼557/581 nm and a Kd of ∼570 nM. The AM ester form has a net positive charge, which promotes sequestration into mitochondria. The probe was dissolved in dimethyl sulfoxide (DMSO) and diluted to a final concentration of 5 μM at the bath. After 30 min of incubation with the dye at room temperature, the preparation was washed with a dye-free solution for 30 min and kept at 28–32°C. The experiments were conducted in the absence of Rhod 2-AM in the extracellular solution. Muscle contractions were prevented by including in the bath 15 μM D-tubocurarine (Sigma-Aldrich).

Nerve electrical stimulation

The nerve was stimulated through a suction electrode. The stimulation consisted of square wave pulses of 0.15 ms duration and 2–40 V amplitude at variable frequencies (0.5–20 Hz) and train durations (5–20 s). Intervals between trains were always ≥10 min unless otherwise stated to allow for complete recovery of the terminal resting values.

Mitochondrial membrane potential essays

The experiments were conducted as those with mitochondrial calcium dyes. The cell-permeant membrane potential dye, rhodamine 123 (Sigma-Aldrich), previously dissolved in DMSO, was used at a working concentration of 0.3 μM at the bath. After 30 min of incubation with the dye, at room temperature, the preparation was washed, and the recording was performed with a solution containing 0.03 μM of the drug. The recordings were done at 28–32°C.

Live imaging acquisition and analysis

Live experiments were conducted at near-physiological temperature (28–32°C) using a temperature controller (TC-344B) connected to a thermistor (SF-28 SloFlo, Warner Instruments). Mitochondrial calcium and exo-endocytosis images were acquired and analyzed similarly unless otherwise stated. Rhod-2 and SypHy were excited with a 488 nm laser line, and emitted fluorescence was monitored with a Yokogawa CSU-X1 spinning disk system (3i, Germany) mounted on an upright BX61WI microscope (Olympus). Images were acquired using a back-thinned EM-CCD camera C9100-13 (Hamamatsu) with an effective number of pixels of 512(H) x 512(V) and a pixel size of 16 x 16 μm. Images were acquired at up to four frames/s with commercial software (SlideBook™ 5.0, 3i). Before analysis, images were aligned using a routine of the SlideBook program. Images were exported to ImageJ for analysis. Regions of interest (ROIs) were outlined with a threshold-based macro routine through the time series, and the data exported to Microsoft Office Excel. The changes in the fluorescence intensity of ROIs were subtracted for the mean background level. Correction for time-dependent loss of signal, mostly due to photobleaching, was performed by subtracting the exponential fits of resting-state fluorescence before and after recovery from the stimuli. The mean intensity of the signal from different ROIs at a given terminal was calculated considering the ROIs size. Fluorescence intensity values were plotted versus time, and different parameters were calculated from the recordings. Resting fluorescence (F_{basal}) was measured as the average fluorescence at the ROI before stimulation. Change in fluorescence was expressed as ΔF ($\Delta F = F - F_{basal}$) or as $\Delta F/F_{basal}$, to obtain the number of folds that the signal changed over baseline fluorescence. To compare the time course of the fluorescence changes (rising and decaying kinetics) $\Delta F/F_{max}$ was calculated. The rise time was calculated as the time from 10 to 90% of the maximum amplitude. The decay time was expressed as the time required for the signal to return to half its peak value ($t_{1/2}$) or to drop 63% of its maximum value (time constant, τ). Calcium influx and efflux rates were calculated as $\Delta F/\Delta t$ for each time point and expressed as $\Delta F/s$. The corrected signals were converted to $[Ca^{2+}]$ using the simplified calibration equation specified in the 'Results' section. Although each ROI was analyzed individually, the characteristics of the different ROIs' responses of the same terminal were usually similar and thus were averaged together. Unless otherwise stated, in the Rhod-2 experiments presented here on the responses that displayed a rapid and relatively large drop component, ≥10% of the maximal amplitude, characteristic of the mixed and cytosolic responses (Supplementary Material, Fig. S2C and D), however, were discarded for later analysis.

Electrophysiology

Synaptic transmission recordings were performed in acute neuromuscular preparations of the TVA muscle at room temperature. A glass microelectrode (10–20 MΩ) filled with 3 M KCl was connected to an intracellular recording amplifier (TEC-05X; npi electronic) and used to impale single muscle fibers near the motor nerve endings. Evoked EPPs and mEPPs were recorded as described previously (7). Muscle contractions were prevented by including in the bath 3–4 μM μ-conotoxin GIIIB (Alomone Laboratories). The mean amplitudes of the EPP and mEPPs recorded at each NMJ were linearly normalized to −70 mV resting membrane potential, and EPPs were corrected for non-linear summation (52, 53).

Immunohistochemistry

TVA muscles from control and SMA mice were fixed (4% paraformaldehyde), washed (0.1 M glycine in PBS) for 30 min, permeabilized (1% (v/v) Triton X-100 in PBS) for 90 min, and incubated in 5% (w/v) BSA, 1% Triton X-100 in PBS for 3 h. Samples were incubated overnight at 4°C with the primary antibodies: monoclonal Syt1 (1:250), rabbit polyclonal Syt2 (1:200) or rabbit polyclonal SV2B (1:200), all from Synaptic Systems. The next day, muscles were incubated in PBS containing 0.05% Triton X-100 for 1 h, exposed to the appropriate secondary antibodies for 1 h (Alexa Fluor 647-conjugated goat anti-rabbit (Invitrogen), or CF488-conjugated donkey anti-mouse (Biotium)), plus 10 ng/ml rhodamine-BTX, and bathed again with 0.05% Triton X-100 for 90 min. Finally, muscles were mounted with Slowfade medium (Invitrogen).

Statistical analysis

Statistical analysis of imaging and electrophysiological data was performed using GraphPad Prism 5 (GraphPad Software). All values mentioned in the text and represented in graphs are averages ± standard errors of the mean (SEM) unless stated otherwise. Parametric statistics were used whenever possible. The assumption of homogeneity of variances was assayed with Levene's test, using $\alpha = 0.05$ as a cut-off. When the distribution was normal statistical comparisons between experimental conditions were made using Student's paired two-tailed *t*-test, or

unpaired *t*-test, as indicated. When the distribution was not normal, the Mann–Whitney rank-sum test was used.

Given that the number of terminals analyzed per condition was typically five or less in some live imaging experiments, every terminal was treated as statistically independent. Results were considered statistically different when the *P*-value was < 0.05. Data in parentheses (*n*, *N*): *n*, the number of nerve terminals (imaging experiments) or muscle fibers (electrophysiological experiments) per group; *N*, number of mice per group. All experiments reported include the results of at least three animals per genotype.

Supplementary Material

Supplementary material is available at *HMG* online.

Acknowledgements

This work was supported by the Spanish Agencia Estatal de Investigación [grant number: PID2019-110272RB-100/ AEI/10.13039/501100011033] and by SMA Europe. We are grateful to Dr. G. Alvarez de Toledo and Dr. Saravanan Arumugam for useful discussions and comments on the manuscript and Mara Guerra and Andrea Fuentes for excellent technical assistance.

References

1. Sugarman, E.A., Nagan, N., Zhu, H. *et al.* (2012) Pan-ethnic carrier screening and prenatal diagnosis for spinal muscular atrophy: clinical laboratory analysis of >72 400 specimens. *Eur. J. Hum. Genet.*, **20**, 27–32.
2. Lefebvre, S., Bürglen, L., Reboullet, S. *et al.* (1995) Identification and characterization of a spinal muscular atrophy-determining gene. *Cell*, **80**, 155–165.
3. Pellizzoni, L., Kataoka, N., Charroux, B. *et al.* (1998) A novel function for SMN, the spinal muscular atrophy disease gene product, in pre-mRNA splicing. *Cell*, **95**, 615–624.
4. Bernabò, P., Tebaldi, T., Groen, E.J.N. *et al.* (2017) In vivo translatome profiling in spinal muscular atrophy reveals a role for SMN protein in ribosome biology. *Cell Rep.*, **21**, 953–965.
5. Ruiz, R., Casañas, J.J., Torres-Benito, L. *et al.* (2010) Altered intracellular Ca^{2+} homeostasis in nerve terminals of severe spinal muscular atrophy mice. *J. Neurosci.*, **30**, 849–857.
6. Kong, L., Wang, X., Choe, D.W. *et al.* (2009) Impaired synaptic vesicle release and immaturity of neuromuscular junctions in spinal muscular atrophy mice. *J. Neurosci.*, **29**, 842–851.
7. Tejero, R., Lopez-Manzaneda, M., Arumugam, S. *et al.* (2016) Synaptotagmin-2, and −1, linked to neurotransmission impairment and vulnerability in spinal muscular atrophy. *Hum. Mol. Genet.*, **25**, 4703–4716.
8. Torres-Benito, L., Neher, M.F., Cano, R. *et al.* (2011) SMN requirement for synaptic vesicle, active zone and microtubule postnatal organization in motor nerve terminals. *PLoS One*, **6**, 26164.
9. Dimitriadi, M., Derdowski, A., Kalloo, G. *et al.* (2016) Decreased function of survival motor neuron protein impairs endocytic pathways. *Proc. Natl. Acad. Sci.*, **113**, E4377–E4386.
10. Hosseinibarkooie, S., Peters, M., Torres-Benito, L. *et al.* (2016) The power of human protective modifiers: PLS3 and CORO1C unravel impaired endocytosis in spinal muscular atrophy and rescue SMA phenotype. *Am. J. Hum. Genet.*, **99**, 647–665.
11. Riessland, M., Kaczmarek, A., Schneider, S. *et al.* (2017) Neurocalcin delta suppression protects against spinal muscular atrophy in humans and across species by restoring impaired endocytosis. *Am. J. Hum. Genet.*, **100**, 297–315.
12. Janzen, E., Mendoza-Ferreira, N., Hosseinibarkooie, S. *et al.* (2018) CHP1 reduction ameliorates spinal muscular atrophy pathology by restoring calcineurin activity and endocytosis. *Brain*, **141**, 2343–2361.
13. Kariya, S., Park, G.H., Maeno-Hikichi, Y. *et al.* (2008) Reduced SMN protein impairs maturation of the neuromuscular junctions in mouse models of spinal muscular atrophy. *Hum. Mol. Genet.*, **17**, 2552–2569.
14. Miller, N., Shi, H., Zelikovich, A.S. *et al.* (2016) Motor neuron mitochondrial dysfunction in spinal muscular atrophy. *Hum. Mol. Genet.*, **25**, 3395–3406.
15. Martinez, T.L., Kong, L., Wang, X. *et al.* (2012) Survival motor neuron protein in motor neurons determines synaptic integrity in spinal muscular atrophy. *J. Neurosci.*, **32**, 8703–8715.
16. Acsadi, G., Lee, I., Li, X. *et al.* (2009) Mitochondrial dysfunction in a neural cell model of spinal muscular atrophy. *J. Neurosci. Res.*, **87**, 2748–2756.
17. Kirichok, Y., Krapivinsky, G. and Clapham, D.E. (2004) The mitochondrial calcium uniporter is a highly selective ion channel. *Nat. Cell Biol.*, **427**, 360–364.
18. Baughman, J.M., Perocchi, F., Girgis, H.S. *et al.* (2011) Integrative genomics identifies MCU as an essential component of the mitochondrial calcium uniporter. *Nature*, **476**, 341–345.
19. De Stefani, D., Raffaello, A., Teardo, E. *et al.* (2011) A forty-kilodalton protein of the inner membrane is the mitochondrial calcium uniporter. *Nature*, **476**, 336–340.
20. Raturi, A. and Simmen, T. (2013) Where the endoplasmic reticulum and the mitochondrion tie the knot: the mitochondria-associated membrane (MAM). *Biochim. Biophys. Acta - Mol. Cell Res.*, **1833**, 213–224.
21. Palty, R., Silverman, W.F., Hershfinkel, M. *et al.* (2010) NCLX is an essential component of mitochondrial Na^{+}/Ca^{2+} exchange. *Proc. Natl. Acad. Sci. U. S. A.*, **107**, 436–441.
22. Tejero, R., Lopez-Manzaneda, M., Franco-Espín, J. *et al.* (2018) Maturation and heterogeneity of vertebrate motor synapses. *Curr. Opin. Physio.*, **4**, 1–6.
23. Janz, R., Goda, Y., Geppert, M. *et al.* (1999) SV2A and SV2B function as redundant Ca^{2+} regulators in neurotransmitter release. *Neuron*, **24**, 1003–1016.
24. Xu, T. and Bajjalieh, S.M. (2001) SV2 modulates the size of the readily releasable pool of secretory vesicles. *Nat. Cell Biol.*, **3**, 691–698.
25. Yao, J., Nowack, A., Kensel-Hammes, P. *et al.* (2010) Cotrafficking of SV2 and synaptotagmin at the synapse. *J. Neurosci.*, **30**, 5569–5578.
26. Miesenböck, G., De Angelis, D.A. and Rothman, J.E. (1998) Visualizing secretion and synaptic transmission with pH-sensitive green fluorescent proteins. *Nature*, **394**, 192–195.
27. Sankaranarayanan, S., De Angelis, D., Rothman, J.E. *et al.* (2000) The use of pHluorins for optical measurements of presynaptic activity. *Biophys. J.*, **79**, 2199–2208.
28. Tabares, L., Ruiz, R., Linares-Clemente, P. *et al.* (2007) Monitoring synaptic function at the neuromuscular junction of a mouse expressing SynaptopHluorin. *J. Neurosci.*, **27**, 5422–5430.
29. Heidelberger, R. (2001) ATP is required at an early step in compensatory endocytosis in synaptic terminals. *J. Neurosci.*, **21**, 6467–6474.
30. Rangaraju, V., Calloway, N. and Ryan, T.A. (2014) Activity-driven local ATP synthesis is required for synaptic function. *Cell*, **156**, 825–835.

31. Talbot, J.D., David, G. and Barrett, E.F. (2003) Inhibition of mitochondrial Ca^{2+} uptake affects phasic release from motor terminals differently depending on external $[Ca^{2+}]$. *J. Neurophysiol.*, **90**, 491–502.
32. Montero, M., Alonso, M.T., Carnicero, E. *et al.* (2000) Chromaffin-cell stimulation triggers fast millimolar mitochondrial Ca^{2+} transients that modulate secretion. *Nat. Cell Biol.*, **2**, 57–61.
33. Babcock, D.F., Herrington, J., Goodwin, P.C. *et al.* (1997) Mitochondrial participation in the intracellular Ca^{2+} network. *J. Cell Biol.*, **136**, 833–844.
34. David, G., Barrett, J.N. and Barrett, E.F. (1998) Evidence that mitochondria buffer physiological Ca^{2+} loads in lizard motor nerve terminals. *J. Physiol.*, **509**, 59–65.
35. David, G. and Barrett, E.F. (2000) Stimulation-evoked increases in cytosolic $[Ca^{2+}]$ in mouse motor nerve terminals are limited by mitochondrial uptake and are temperature-dependent. *J. Neurosci.*, **20**, 7290–7296.
36. David, G., Talbot, J. and Barrett, E.F. (2003) Quantitative estimate of mitochondrial $[Ca^{2+}]$ in stimulated motor nerve terminals. *Cell Calcium*, **33**, 197–206.
37. Grynkiewicz, G., Poenie, M. and Tsien, R.Y. (1985) A new generation of Ca^{2+} indicators with greatly improved fluorescence properties. *J. Biol. Chem.*, **260**, 3440–3450.
38. David, G. (1999) Mitochondrial clearance of cytosolic Ca^{2+} in stimulated lizard motor nerve terminals proceeds without progressive elevation of mitochondrial matrix $[Ca^{2+}]$. *J. Neurosci.*, **19**, 7495–7506.
39. Chalmers, S. and Nicholls, D.G. (2003) The relationship between free and total calcium concentrations in the matrix of liver and brain mitochondria. *J. Biol. Chem.*, **278**, 19062–19070.
40. Kostic, M., H.R., L. M., Hilmar, B., *et al.* (2015) PKA phosphorylation of NCLX reverses mitochondrial calcium overload and depolarization, promoting survival of PINK1- deficient dopaminergic neurons. *Cell Rep.*, **13**, 376–386.
41. Zoccarato, F. and Nicholls, D. (1982) The role of phosphate in the regulation of the independent calcium-efflux pathway of liver mitochondria. *Eur. J. Biochem.*, **127**, 333–338.
42. Nguyen, K.T., García-Chacón, L.E., Barrett, J.N. *et al.* (2009) The Ψ m depolarization that accompanies mitochondrial Ca^{2+} uptake is greater in mutant SOD1 than in wild-type mouse motor terminals. *Proc. Natl. Acad. Sci.*, **106**, 2007–2011.
43. Tejero, R., Balk, S., Franco-Espin, J. *et al.* (2020) R-roscovitine improves motoneuron function in mouse models for spinal muscular atrophy. i*Science*, **23**, 100826.
44. David, G. and Barrett, E.F. (2003) Mitochondrial Ca^{2+} uptake prevents desynchronization of quantal release and minimizes depletion during repetitive stimulation of mouse motor nerve terminals. *J. Physiol.*, **548**, 425–438.
45. García-Chacón, L.E., Nguyen, K.T., David, G. *et al.* (2006) Extrusion of Ca^{2+} from mouse motor terminal mitochondria via a Na^{+}-Ca^{2+} exchanger increases post-tetanic evoked release. *J. Physiol.*, **574**, 663–675.
46. Damiano, M., Starkov, A.A., Petri, S. *et al.* (2006) Neural mitochondrial Ca^{2+} capacity impairment precedes the onset of motor symptoms in G93A Cu/Zn-superoxide dismutase mutant mice. *J. Neurochem.*, **96**, 1349–1361.
47. Jablonka, S., Beck, M., Lechner, B.D. *et al.* (2007) Defective Ca^{2+} channel clustering in axon terminals disturbs excitability in motoneurons in spinal muscular atrophy. *J. Cell Biol.*, **179**, 139–149.
48. Nicholls, D.G. and Chalmers, S. (2004) The integration of mitochondrial calcium transport and storage. *J. Bioenerg. Biomembr.*, **36**, 277–281.
49. McCormack, J.G., Halestrap, A.P. and Denton, R.M. (1990) Role of calcium ions in regulation of mammalian intramitochondrial metabolism. *Physiol. Rev.*, **70**, 391–425.
50. Jouaville, L.S., Pinton, P., Bastianutto, C. *et al.* (1999) Regulation of mitochondrial ATP synthesis by calcium: evidence for a long-term metabolic priming. *Proc. Natl. Acad. Sci. U. S. A.*, **96**, 13807–13812.
51. Hsieh-Li, H.M., Chang, J.-G., Jong, Y.-J. *et al.* (2000) A mouse model for spinal muscular atrophy. *Nat. Genet.*, **24**, 66–70.
52. McLachlan, E.M. and Martin, A.R. (1981) Non-linear summation of endplate potentials in the frog and mouse. *J. Physiol.*, **311**, 307–324.
53. Ruiz, R., Cano, R., Casañas, J.J. *et al.* (2011) Active zones and the readily releasable pool of synaptic vesicles at the neuromuscular junction of the mouse. *J. Neurosci.*, **31**, 2000–2008.